Desalination and Water Treatment
www.deswater.com
doi: 10.5004/dwt.2022.28767

270 (2022) 35–43
September

Experimental study of different shape droplet oblique impact on a thin liquid film

Minle Bao[a], Feng Wang[b], Luyuan Gong[a,*], Yali Guo[a,*], Shengqiang Shen[a]

[a]*Key Laboratory of Ocean Energy Utilization and Energy Conservation of Ministry of Education, Dalian University of Technology, Dalian, China, emails: lygong@dlut.edu.cn (L. Gong), ylguo@dlut.edu.cn (Y. Guo), baoml@mail.dlut.edu.cn (M. Bao), zzbshen@dlut.edu.cn (S. Shen)*
[b]*GD Midea Heating & Ventilating Equipment Co., Ltd., Foshan, China, email: wang_dlut@foxmail.com (F. Wang)*

Received 18 February 2022; Accepted 23 July 2022

ABSTRACT

Experiments of a single droplet oblique impact on a thin liquid film are carried out. In the experiments, the impact angle is adjusted by varying a horizontal airflow, and three typical initial droplet shapes of the sphere, horizontal spheroid, and vertical spheroid are selected. Effects of impact angle, initial droplet shape, and film thickness on the impact outcomes are mainly studied. Results show that the liquid crown seems to be a beveled round tube in the case of sphere droplet impact. In contrast, it seems to be a ship in the case of vertical spheroid droplet impact, and the liquid crown is less asymmetry for the horizontal spheroid droplet impact. When the Weber number exceeds the critical value, secondary droplets will detach from the rim of the liquid jets. The number and size of the secondary droplets are associated with the impact droplet shapes. For the sphere droplet impact case, the crown radius and the crown height on the front side of the advancing droplet (right side) increase with the impact angle. With an increase in the film thickness, the right crown radius decreases, while the right crown height first increases and then decreases.

Keywords: Droplet impact; Thin liquid film; Impact angle; Droplet shapes

1. Introduction

The dynamics of droplet impact on a liquid surface is an interesting phenomenon, especially the temporal evolution of the crown lamella and the splashing. It widely exists in nature and industrial applications, such as raindrops impact on the ground or the crop leaves, automized oil injection in combustion chambers, ink droplets adhering to the target substrate in inkjet printing equipment, low-temperature droplets impact on the heat exchange tube of the falling film evaporator equipped in desalination and refrigeration fields, fire extinguish and spray cooling [1–4]. During these fields, the droplet generally impacts the liquid surface from various angles, like the wind-driven raindrop impact and spray droplet impact. Therefore, the research on the dynamics of oblique droplet impact is significantly important. For the oblique impact case, the droplet will deform in the air due to the gravity, drag force, and even the wind force [5,6]. However, few experiments have been conducted to investigate the dynamic characteristics of oblique droplet impact on a liquid film. Before proceeding with this work, the previous relevant research that inspires the present investigation is reviewed first.

For the normal impact of a droplet on a stationary liquid surface, three typical outcomes usually occur, including deposition, crown formation without splashing, and crown formation with splashing [7,8]. The impact outcome mainly depends on the impact velocity (v), droplet diameter (d), and dimensionless film thickness ($h^* = h/d$), where h is the film thickness. According to the article reviewed

* Corresponding authors.

by Liang and Mudawar [9], the impact target is generally classified as a thin film, liquid film, shallow pool, and deep pool, and the classification criteria are different in previous research. In particular, the thin liquid film is restricted to $h^* < 1$, as reported by Cossali et al. [10] and Motzkus et al. [11] After the droplet impacts the liquid film, a thin liquid sheet ejects from the neck region between the droplet and the liquid film, and then grows into a liquid crown [12,13]. Jets form at the rim of the liquid crown and may break up into secondary droplets due to the Rayleigh–Taylor instability [14,15]. Moreover, capillary waves form around the impact region [16,17].

Research on crown evolution mainly focuses on the measurements of the crown diameter and crown height [18,19]. Weber number (We) and Reynolds number (Re) are the main dimensionless parameters that govern splashing, which can be expressed as follows:

$$We = \frac{\rho d v^2}{\sigma} \tag{1}$$

$$\mathrm{Re} = \frac{\rho d v}{\mu} \tag{2}$$

where ρ is the liquid density, σ is the surface tension coefficient, and μ is the liquid viscosity. A constant parameter K associated with the We and Re is generally adopted as the splashing threshold [20]. Li et al. [21] measured the number and the size of the secondary droplets using a high-speed camera and a developed particle tracking algorithm. They found that the number of the secondary droplets and the peak of the diameter distribution increase with the Weber number, and the film thickness has little effect on the number of the secondary droplets.

Compared to the investigation of normal impact mentioned above, the oblique impact of a droplet on a thin liquid film has received little attention in recent years. Also, an obvious difference in the oblique impact is that the flow features are asymmetrical. Leneweit et al. [22] experimentally studied the oblique impact of a single droplet on a liquid pool with We ranging from 15 to 249 and impact angle (θ) ranging from 5.4° to 64.4°. The θ is defined as the angle between the velocity vector of the droplet and the normal vector to the liquid film. The normal component of Weber number (We_n) is adopted to classify the morphological evolution. Formation of the capillary wave, lamella, and partial immersion are reported and discussed deeply. Okawa et al. [5] investigated the effect of impact angle and film thickness on the deposition-splashing limit. Measurement of the total mass of secondary droplets was reported, and results indicated that the total mass of the secondary droplets remarkably increases with the impact angle when $\theta < 50°$. Concerning the oblique impact of a small droplet with a diameter of 100 μm on a deep liquid pool, Gielen et al. [23] conducted the experimental study to quantify the cavity and the splashing threshold. Three different impact regimes of deposition, single-sided splashing, and omni-directional splashing, are identified by accounting for the impact angle and the Weber number. By adding a wind field, Liu [6] experimentally investigated the oblique impact of a droplet on a deep-water pool, in which the wind speed could be adjusted to vary the impact angle and the impact velocity. The results recorded the formation of the asymmetrical crown on the leeward of the impact region, the swelled wave on the windward side, and the evolution of the ligaments. The effects of the droplet diameter and wind speed on the evolution of the cavity and the central jet were measured in Liu's new work [24]. In this new study, they found that the effect of wind on the penetration depth of the cavity is very small at the initial stage of the cavity expansion, while the maximum central jet height is drastically associated with the wind. According to the references [6,24], it should be noted that the impact of a droplet on a liquid surface in the presence of wind is the same as the oblique droplet impact.

In the last two decades, many scholars have done exploratory work on the microscopic features of oblique droplet impact in the aspect of numerical simulation, benefiting from the fast growth of computer technology. Cheng and Lou [25] applied the Lattice Boltzmann method (LBM) to demonstrate the differences between the splashing behavior of the oblique droplet impact on a moving wall and a stationary wall. Using the moment-of-fluid (MOF) method, Guo and Lian [26] investigated the effect of impact angle on high-speed drop oblique impact and found that the increasing tangential velocity leads to a reduction in lamella height and radius on the side behind the advancing drop. Guo et al. [27] and Wang et al. [28] employed the coupled level set and volume of fluid (CLSVOF) method to simulate droplet oblique impact. According to their results, the crown radiuses on both sides of the advancing droplet show an opposite variation tendency as the impact angle increases. Chen et al. [29] numerically studied the splashing dynamics of the oblique drop impact on the thin film by utilizing the lattice Boltzmann flux solver associated with the diffuse interface method. Bao et al. [30] simulated the interface evolution characteristics of dual droplets successive oblique impact on a thin liquid film and found some interesting interface features during the collision and coalescence of crowns.

From the above reviews on oblique droplet impact, we noted that the most impact target is the liquid pool, and few studies concern the effect of droplet shapes. Moreover, few experiments of oblique droplet impact have been conducted to quantify the crown evolution. Since the deformation of impact droplets widely exists in nature and industry, like the cases of the wind-driven raindrop impact and the spray droplet impact, a study of different shape droplet impact is necessary. In this study, outcomes after the oblique impact of a single droplet with three different shapes on a thin liquid film are presented experimentally. In addition, the effects of impact angle and film thickness on the crown evolution are quantified.

2. Experimental apparatus and measurement method

The schematic of the experimental apparatus with two view directions is shown in Fig. 1. The main components include a droplet generator with a syringe and a needle to produce droplets under the control of pressure, a horizontal airflow produced by a fan and uniformed by a flow equalizing plate, a water tank with an inside test platform to

produce a thin liquid film, a high-speed camera with a backlight to record the impact outcomes, a light diffuser, and a data acquisition computer.

A single droplet can be formed at the flat-tipped needle by imposing the liquid in the syringe under the control of a Kruss DSA 30 system. The droplet will detach when its gravity exceeds the surface tension force and then falls freely. The normal component velocity of the droplet can be adjusted by varying the height of the needle. The airflow away from the liquid film surface adds a horizontal velocity to the falling droplet. Thus, the droplet will impact the liquid film obliquely. The liquid film is prepared by depositing liquid in the water tank to ensure that the liquid film on the test platform is flat and thin. The film thickness is varied by changing the liquid volume. It should be emphasized that the surface size of the test platform (30 mm × 40 mm) is large enough in the present study that the impact outcomes are not disturbed by the liquid around the test platform. The materials of the droplet and liquid film are water. The experiment is carried out at room temperature. The physical parameters of the liquid and surrounding gas at room temperature are shown in Table 1. The impact outcomes are recorded by a high-speed camera (Phantom v641) at 2500 frames/s, equipped with a 100 mm, f-2.8 Tokina macro lens. For a better view of the overall crown outline, the camera is aligned to the impact surface and inclined at an angle of 35º to the horizontal plane. Each image has a resolution of 1,280 × 720. A xenon lamp with a diffuser in front is used as the backlight to expose the images. The light diffuser is placed between the xenon lamp and the liquid film to uniform the backlight.

In this study, all measurements obtained from the acquired images are calculated by pixel analysis, which is performed by using the commercial software LabVIEW, and calibration is performed by comparing a reference of known size. Image distortion caused by the shooting angle will be corrected. Fig. 2 shows the geometric model of three typical droplet shapes. Droplet equivalent diameter (d) is calculated using its horizontal diameter (d_h) and vertical diameter (d_v) [31], which can be expressed as

$$d = \left(d_h^2 d_v\right)^{\frac{1}{3}} \tag{3}$$

The equivalent diameter in the case without airflow is about 3 mm, with an error of 0.03 mm. The v and θ can be adjusted by varying the horizontal airflow and the height of the needle and calculated from the droplet positions recorded in the two images at a time interval of 0.5 ms prior to the impact. Due to the gravity, wind power, and drag force, the droplet will rotate and deform in the wind field, resulting in the measurement errors of v and θ up to 3% and 2°, respectively. The test surface is titanium with an average surface roughness of less than 0.05 μm.

The initial impact time is defined as t = 0 ms when the droplet just contacts the liquid film. Since the droplet will rotate and deform in the wind field, three typical initial droplet shapes of the sphere, horizontal spheroid, and vertical spheroid, will be mainly discussed, as the geometric model shown in Fig. 2. The three typical droplets are defined by the ratio of d_h to d_v, referred to as s-droplet, hs-droplet, and vs-droplet, respectively, corresponding to $0.9 < d_h/d_v < 1.1$, $d_h/d_v > 1.2$, and $d_h/d_v < 0.8$.

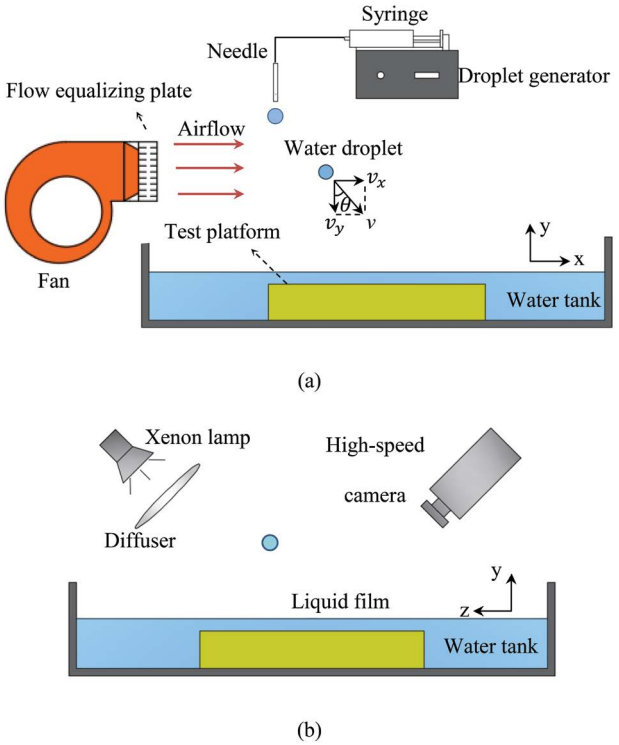

Fig. 1. Schematic of the experimental apparatus with two view directions: (a) front view and (b) side view.

The experiments were repeated three times for each experimental condition. According to the Laiyite criterion (3σ criterion), the abnormal data are detected and eliminated correctly prior to the analysis. When the experimental values measured are x_1, x_2, … and x_n, the average value ($\bar{x}$), residual (ε_i), and standard deviation ($s(x_i)$) can be expressed as:

$$\bar{x} = \frac{1}{n}\sum_{i=1}^{n} x_i \tag{4}$$

$$\varepsilon_i = x_i - \bar{x} \tag{5}$$

$$s\left(x_i\right) = \sqrt{\frac{1}{n-1}\sum_{i=1}^{n}\left(x_i - \bar{x}\right)^2} \tag{6}$$

where n is the total number of the experimental values measured in each experiment, and i is the serial number of the experimental values measured. If the absolute value of the residue of an experimental value satisfies $|\varepsilon_i| > 3\, s(x_i)$, this value is the outlier and should be removed. The average value of the three experiments was calculated as the final experimental result.

3. Results and discussion

In this section, we first quantitatively investigate the effects of initial droplet shape on the crown and splashing evolution. Then we present the time evolution of the crown

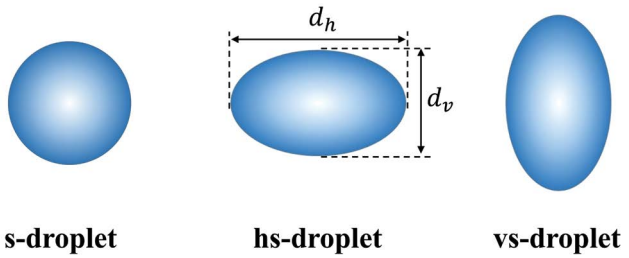

Fig. 2. Geometric model of three typical droplet shapes.

lamella in the case of the s-droplet impact, considering the effects of the impact angle and the film thickness.

3.1. Outcomes after impact

The outcomes of three typical droplets of the sphere, vertical spheroid, and horizontal spheroid impact on liquid film are shown in Fig. 3, where the dimensionless film thickness is 0.33. It can be seen that the droplet shortly merges with the liquid film after impact, during which the impacting droplet squeezes the liquid film to form a liquid crown, as shown at t = 2 ms. The crown then extends outside as time increases. Fig. 3 also shows that the impact outcomes have a strong dependence on the initial droplet shape.

For the s-droplet impact, due to the horizontal component velocity, the crown lamella on the front side of the advancing droplet (right side) increases more quickly than that on the behind side of the advancing droplet (left side), resulting in an asymmetrical crown feature along the airflow direction. As shown at t = 2 and 4 ms, the liquid crown seems to be a beveled round tube. At t = 2 ms, as the right crown lamella grows so fast that the upper edge of the crown lamella appears to be unstable, and some small jets emerge. The crown jets at the right side enlarge with time, but no secondary droplets appear. It can be noticed that the crown edge on the left side is almost smooth until it absolutely merges into the film at t = 10 ms. The left crown height increases till t = 4 ms and then begins to decrease. As the left crown lamella falls back to the liquid film, the liquid film near the outside of the left crown will be squeezed, and thus capillary waves appear on the left side, as shown at t = 8 ms. The capillary waves spread out with time, and they become more obvious when the left crown merges with the liquid film at t = 10 ms.

For the vs-droplet impact, as shown in Fig. 3b, a ship-like crown forms shortly after impact at t = 2 ms. When the lower part of the vs-droplet begins to contact the liquid film, the remaining part keeps moving to the right because of the inertia force, resulting in a ship-like crown with a cuspate prow. Different from the s-droplet impact, no jets emerge, and the upper edge of the whole crown lamella is almost smooth during the vs-droplet impact. The crown height on the left side increases first, then decreases, and even almost entirely merges into the liquid film at t = 10 ms, which is similar to the process in the above s-droplet impact case. However, the prow of the ship-like crown (crown lamella on the right side) has been enlarging in the time range of this study. Capillary waves can be clearly observed on the left side at t = 10 ms.

For the hs-droplet impact, as shown in Fig. 3c, the effect of airflow on the impacting droplet is smaller due to a smaller windward area. Therefore, the crown dynamics are less asymmetry along the airflow direction compared to the above two cases. Several small jets emerge on the upper edge of the crown lamella at t = 2 ms, then enlarge with time and even merge together. As marked in Fig. 3c, the adjacent jets of 1 and 2(t = 4 ms) merge into a new large jet of 3(t = 8 ms). In contrast, the portion of the crown lamella on the left side is smooth without ejecting jets.

Fig. 4 shows the outcomes of three typical droplets impacting a thin liquid film, where the film thickness and the horizontal component velocity of the droplet are the same as the cases shown in Fig. 3, but the normal component velocity of the droplet is larger, which means that the droplets in the following cases have a larger Weber number and a smaller impact angle. Compared to the cases shown in Fig. 3, an obvious difference shown in Fig. 4 is the detachment of the secondary droplets. As shown in Fig. 4, the number and size of the secondary droplets are associated with the droplet shapes. For the s-droplet impact, shown in Fig. 4a at t = 2 ms, small jets emerge at the upper edge of the right crown lamella because of the instability. Those small jets enlarge with time and break up to produce several secondary droplets at t = 10 ms with dimensionless diameters ($d^*_s = d_s/d$) up to 0.38, where d_s is the diameter of the secondary droplet, while as mentioned above in Fig. 3a, the Weber number is too small to separate the secondary droplets, and no secondary droplets appear. At t = 10 ms, crown lamella has totally merged into the liquid film with capillary waves around it. For the vs-droplet, shown in Fig. 4b, the height of the middle part of the crown lamella is less than that of the left and right parts at t = 4ms, and the middle part of the crown lamella first merges with the liquid film at t = 6 ms, followed by the crown lamella on the left side at t = 10ms, obviously different to the vs-droplet impact case shown in Fig. 3b. As

Table 1
Physical properties of liquid and surrounding gas

	Liquid	Surrounding gas
Material	Water	Air
Density ρ (kg/m^3)	998.2	1.225
Dynamic viscosity μ (Pa·s)	1.003×10^{-3}	1.789×10^{-5}
Pressure P (Pa)	–	101,325
Liquid–gas surface tension coefficient σ (N/m)	0.0728	

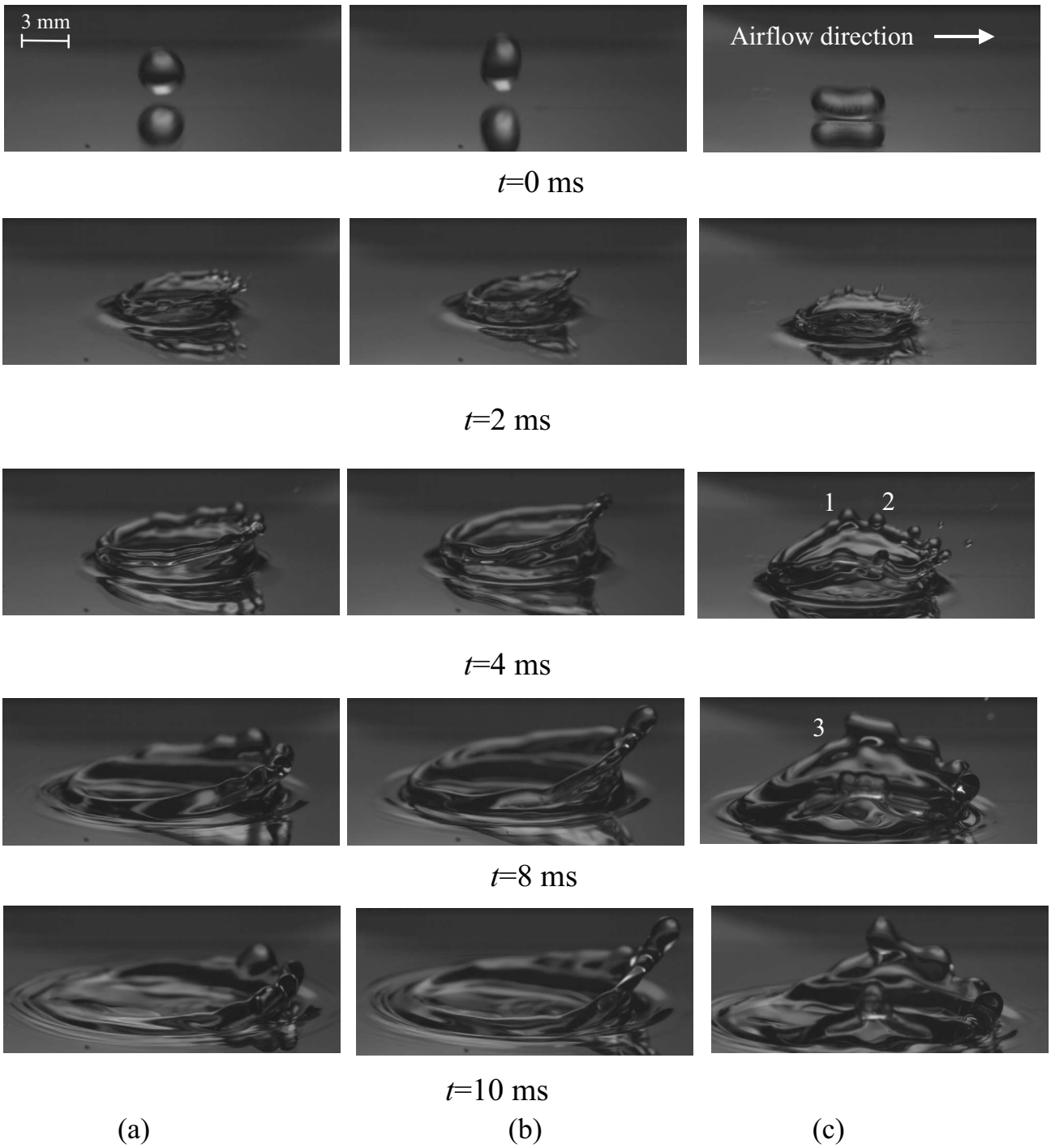

Fig. 3. Typical time series of oblique droplet impact on a thin liquid film: (a) s-droplet impact case (d_h/d_v = 1.02, We = 243, θ = 20.2°), (b) vs-droplet impact case (d_h/d_v = 0.65, We = 249, θ = 21.1°), and (c) hs-droplet impact case (d_h/d_v = 2.3, We = 238, θ = 19.3°).

marked in Fig. 4b at t = 10 ms, a single secondary droplet with a dimensionless diameter of 0.44 detaches from the rim of the prow. For the hs-droplet, the evolution process is basically similar to that shown in Fig. 3c. As marked in Fig. 4c, two pairs of adjacent jets (1, 2, and 1′, 2′) emerge on the upper edge of the crown lamella at t = 2 ms. These jets enlarge with time and finally merges into two large new jets at t = 6 ms, marked as 3 and 3′, respectively. As shown at t = 10 ms, two secondary droplets with a diameter of 0.43 and 0.51 break away from the merged jets.

3.2. Effect of impact angle

In order to quantify the impact outcomes, the right crown radius (R_r) and right crown height (H_r) are adopted as the parameters. The definition of these parameters are

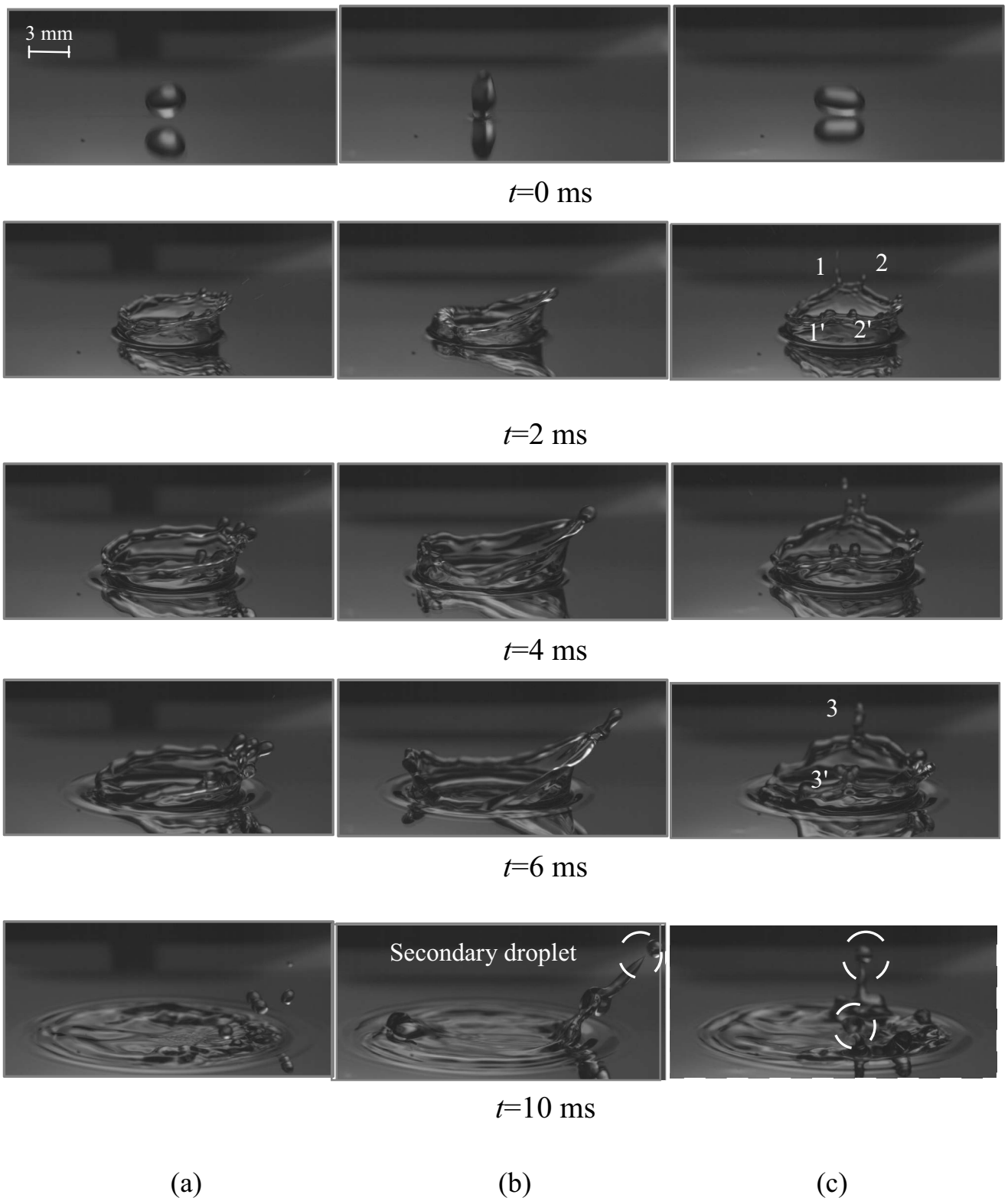

Fig. 4. Typical time series of oblique droplet impact on a thin liquid film: (a) s-droplet impact case (d_h/d_v = 1.1, We = 356, θ = 12.3°), (b) vs-droplet impact case (d_h/d_v = 0.5, We = 342, θ = 11.9°), and (c) hs-droplet impact case (d_h/d_v = 1.7, We = 350, θ = 12.1°).

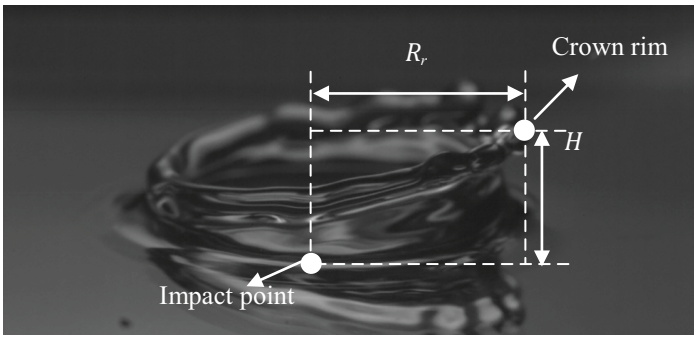

Fig. 5. Sketch of crown lamella with the definition of different geometric parameters.

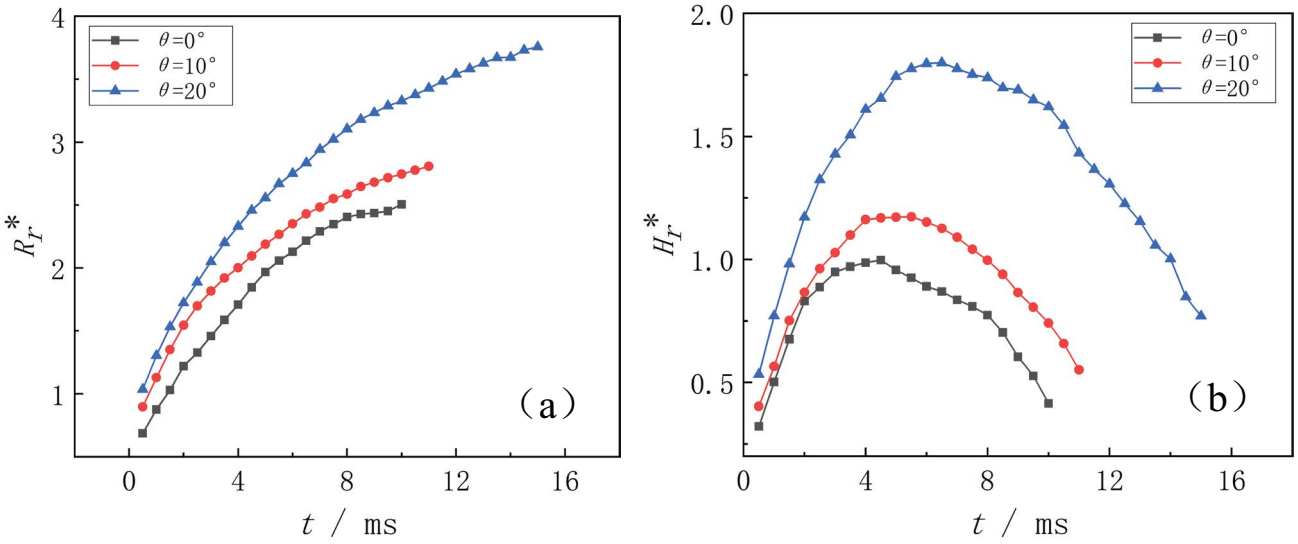

Fig. 6. Time evolution of (a) the right crown radius and (b) right crown height at different impact angles.

shown in Fig. 5, the corresponding dimensionless parameters of which can be expressed as

$$R_r^* = \frac{R_r}{d} \tag{7}$$

$$H_r^* = \frac{H_r}{d} \tag{8}$$

The measurement of the left crown lamella is neglected in this work because of its minor change. For each condition, the average of data measured three times is used to guarantee precision. In the following sections, the droplets will detach from the needle at the same height to obtain the same normal component velocity. In addition, only the initial impact droplets with a sphere shape are adopted. The relative error of the impact angle for each group is less than 5%, the film thickness is less than 1%, and d_h/d_v is less than 5%.

Fig. 6 shows the time evolution of the right crown lamella at different impact angles.After the droplet impact, part of the energy from the droplet will be used for the spread of the liquid crown, and the other part will be converted into the gravity potential energy of the crown to make the crown lamella grow upward. However, when the impact energy is not enough to maintain the rise of the crown lamella, the lamella will fall back to the liquid film because of gravity. Therefore, as shown in Fig. 6, it can be found that the right crown radius increases with time, while the right crown height first increases to a maximum value and then decreases. The increase of impact angle can lead to the rise of horizontal component velocity and kinetic energy, so the right crown radius and the right crown height increase with the impact angle. In Fig. 6b, the case at θ = 0° first reaches its maximum dimensionless crown height of 1 at t = 4.5 ms, followed by the case at 10° with a maximum value of 1.17 at t = 5.5 ms, and finally the case at 20° with a maximum value of 1.8 at t = 6.5 ms.

3.3. Effect of film thickness

Fig. 7 demonstrates the effect of film thickness on the right crown lamella. As shown in Fig. 7a, the right crown radius decreases with the increase of the film thickness. This is because the resistance to the spreading crown lamella will increase with a thicker liquid film. It also can be noted

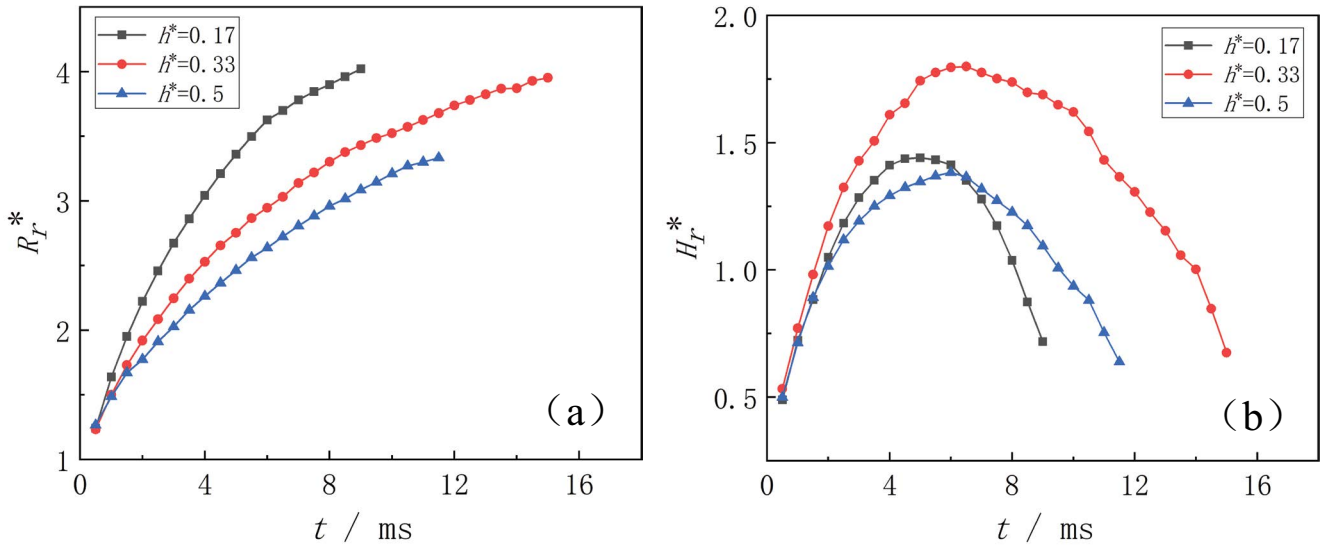

Fig. 7. Time evolution of (a) the right crown radius and (b) right crown height at different film thicknesses.

that the discrepancies between curves corresponding to different film thicknesses are lessened as the film thickness increases. Taking t = 4 ms as an example, when the film thickness increases from 0.17 to 0.33, the right crown radius decreases about 20.3 %, while it decreases about 11.8% as the film thickness increases from 0.33 to 0.5.

As shown in Fig. 7b, the right crown height increases when the h^* increases from 0.17 to 0.33. However, it begins to decrease as the h^* increases from 0.33 to 0.5, and the height for h^* = 0.5 is even lower than that for h^* = 0.17 before 6.5 ms. As the h^* increases from 0.33 to 0.5, part of the impact energy will be transferred to the deeper position in the liquid film. The impact energy for different cases is the same. Therefore, the energy used to support the growth of the crown lamella will be less, leading to the decrease of the right crown height when the h^* increases from 0.33 to 0.5. Although a thinner liquid film means lower resistance, the liquid film is so thin that less liquid can be supplied to maintain the growth of the crown lamella upward when the h^* decreases from 0.33 to 0.17. Therefore, the right crown height is lower at h^* = 0.17 compared to that at h^* = 0.33. According to the variation trend that right crown height first increases with the increase of h^* from 0.17 to 0.33 and then decreases from 0.33 to 0.5, we can indicate that there exists a critical value of h^* between 0.17 and 0.5. A similar conclusion can be noticed in the present numerical research [32]. From Fig. 7b, a meeting point (h^*_r = 1.37 at t = 6.5 ms) can be noticed between the curves of h^* = 0.17 and h^* = 0.5. Before the meeting point, the right crown height is larger at h^* = 0.17 than that at h^* = 0.5. However, after the meeting point, the right crown height at h^* = 0.17 turns lower than that at h^* = 0.5. It is because that the right crown height at h^* = 0.17 increases faster than that at h^* = 0.5 before it reaches the maximum value due to the less film resistance, while the growth of the right crown lamella is also limited by the thinner liquid film at h^* = 0.17 for the lack of enough liquid and the right crown height begins to decreases earlier than that at h^* = 0.5. Then, a meeting point appears.

4. Conclusions

In this study, outcomes of three typical droplets of the sphere, vertical spheroid, and horizontal spheroid obliquely impact on a thin liquid film are visualized using a high-speed camera. A series of experiments are performed with varying initial droplet shape, impact angle, Weber number, and film thickness. For the sphere droplet impact case, measurements of the crown height and radius on the front side of the advancing droplet (right side) are conducted. The brief conclusions are as follows:

- The liquid crown seems to be a beveled round tube in the case of sphere droplet impact, while it seems to be a ship with a cuspate prow in the case of vertical spheroid droplet impact, and the liquid crown is less asymmetry for the horizontal spheroid droplet impact.
- With a smaller Weber number and a larger impact angle, the crown lamella on the behind side of the advancing droplet (left side) first merges with the liquid film regardless of the droplet shape. However, with a larger Weber number and a smaller impact angle, the middle part of the crown lamella first merges with the liquid film in the case of vertical spheroid droplet impact.
- When the Weber number exceeds the critical value, secondary droplets detach from the rim of the jets. The number and size of secondary droplets are related to the impact droplet shapes.
- The right crown radius and right crown height increase with the impact angle, and a larger impact angle leads to a larger maximum right crown height.
- The right crown radius decreases with the increase of the film thickness, while the right crown height increases when the dimensionless film thickness increases from 0.17 to 0.33, and then it begins to decrease as the dimensionless film thickness increases from 0.33 to 0.5.

Acknowledgement

The authors are grateful for the support of the National Natural Science Foundation of China (No. 51936002) and the Fundamental Research Funds for the Central Universities (DUT21LAB128).

References

[1] J.D. Benther, J.D. Pelaez-Restrepo, C. Stanley, G. Rosengarten, Heat transfer during multiple droplet impingement and spray cooling: review and prospects for enhanced surfaces, Int. J. Heat Mass Transfer, 178 (2021) 121587, doi: 10.1016/j.ijheatmasstransfer.2021.121587.
[2] K. Zhao, Y. Wang, Y. Ding, Y. Jiang, Numerical and theoretical study on the spreading characteristics of droplet impact on a horizontal flowing liquid film, Colloids Surf., A, 616 (2021) 126338, doi: 10.1016/j.colsurfa.2021.126338.
[3] M. Bao, F. Wang, Y. Guo, L. Gong, S. Shen, Experimental study of two-phase heat transfer of droplet impact on liquid film, Phys. Fluids, 34 (2022) 042119, doi: 10.1063/5.0089961.
[4] G. Liang, L. Li, L. Chen, S. Zhou, S. Shen, Impact of droplet on flowing liquid film: experimental and numerical determinations, Int. Commun. Heat Mass Transfer, 126 (2021) 105459, doi: 10.1016/j.icheatmasstransfer.2021.105459.
[5] T. Okawa, T. Shiraishi, T. Mori, Effect of impingement angle on the outcome of single water drop impact onto a plane water surface, Exp. Fluids, 44 (2008) 331–339.
[6] X. Liu, Experimental study of drop impact on deep-water surface in the presence of wind, J. Phys. Oceanogr., 48 (2018) 329–341.
[7] R. Rioboo, C. Bauthier, J. Conti, M. Voué, J. De Coninck, Experimental investigation of splash and crown formation during single drop impact on wetted surfaces, Exp. Fluids, 35 (2003) 648–652.
[8] T. Okawa, T. Shiraishi, T. Mori, Production of secondary drops during the single water drop impact onto a plane water surface, Exp. Fluids, 41 (2006) 965–974.
[9] G. Liang, I. Mudawar, Review of mass and momentum interactions during drop impact on a liquid film, Int. J. Heat Mass Transfer, 101 (2016) 577–599.
[10] G.E. Cossali, A. Coghe, M. Marengo, The impact of a single drop on a wetted solid surface, Exp. Fluids, 22 (1997) 463–472.
[11] C. Motzkus, F. Gensdarmes, E. Géhin, Parameter study of microdroplet formation by impact of millimetre-size droplets onto a liquid film, J. Aerosol Sci., 40 (2009) 680–692.
[12] Y. Guo, L. Wei, G. Liang, S. Shen, Simulation of droplet impact on liquid film with CLSVOF, Int. Commun. Heat Mass Transfer, 53 (2014) 26–33.
[13] M. Xu, C. Wang, S. Lu, Water droplet impacting on burning or unburned liquid pool, Exp. Therm. Fluid Sci., 85 (2017) 313–321.
[14] R.L. Vander Wal, G.M. Berger, S.D. Mozes, Droplets splashing upon films of the same fluid of various depths, Exp. Fluids, 40 (2006) 33–52.
[15] Š. Šikalo, E.N. Ganić, Phenomena of droplet–surface interactions, Exp. Therm. Fluid Sci., 31 (2006) 97–110.
[16] N.E. Ersoy, M. Eslamian, Phenomenological study and comparison of droplet impact dynamics on a dry surface, thin liquid film, liquid film and shallow pool, Exp. Therm. Fluid Sci., 112 (2020) 109977, doi: 10.1016/j.expthermflusci.2019.109977.
[17] Z. Che, O.K. Matar, Impact of droplets on liquid films in the presence of surfactant, Langmuir, 33 (2017) 12140–12148.
[18] H. Zhang, J. Li, Q. Liu, Experiment study of droplet impacting on a static hemispherical liquid film, Exp. Comput. Multiphase Flow, 2 (2020) 247–254.
[19] X. Gao, R. Li, Impact of a single drop on a flowing liquid film, Phys. Rev. E, 92 (2015) 053005, doi: 10.1103/PhysRevE.92.053005.
[20] H.M. Kittel, I.V. Roisman, C. Tropea, Splash of a drop impacting onto a solid substrate wetted by a thin film of another liquid, Phys. Rev. Fluids, 3 (2018) 73601, doi: 10.1103/PhysRevFluids.3.073601.
[21] J. Li, H. Zhang, Q. Liu, Characteristics of secondary droplets produced by a single drop impacting on a static liquid film, Int. J. Multiphase Flow, 119 (2019) 42–55.
[22] G. Leneweit, R. Koehler, K.G. Roesner, G. Schäfer, Regimes of drop morphology in oblique impact on deep fluids, J. Fluid Mech., 543 (2005) 303–331.
[23] M.V. Gielen, P. Sleutel, J. Benschop, M. Riepen, V. Voronina, C.W. Visser, D. Lohse, J.H. Snoeijer, M. Versluis, H. Gelderblom, Oblique drop impact onto a deep liquid pool, Phys. Rev. Fluids, 2 (2017) 083602, doi: 10.1103/PhysRevFluids.2.083602.
[24] X. Liu, A. Wang, S. Wang, D. Dai, Effects of wind on the dynamics of the central jet during drop impact onto a deep-water surface, Phys. Rev. Fluids, 3 (2018) 053602, doi: 10.1103/PhysRevFluids.3.053602.
[25] M. Cheng, J. Lou, A numerical study on splash of oblique drop impact on wet walls, Comput. Fluids, 115 (2015) 11–24.
[26] Y. Guo, Y. Lian, High-speed oblique drop impact on thin liquid films, Phys. Fluids, 29 (2017) 082108, doi: 10.1063/1.4996588.
[27] Y. Guo, F. Wang, L. Gong, S. Shen, Numerical study of oblique droplet impact on a liquid film, Eur. J. Mech. B. Fluids, 85 (2021) 386–396.
[28] F. Wang, L. Gong, S. Shen, Y. Guo, Flow and heat transfer characteristics of droplet obliquely impact on a stationary liquid film, Numer. Heat Transfer, Part B, 77 (2020) 228–241.
[29] Z. Chen, C. Shu, Y. Wang, L.M. Yang, Oblique drop impact on thin film: splashing dynamics at moderate impingement angles, Phys. Fluids, 32 (2020) 033303, doi: 10.1063/5.0004142.
[30] M. Bao, Y. Guo, L. Gong, S. Shen, Interface evolution characteristics of dual droplet successive oblique impact on liquid film, Phys. Fluids, 34 (2022) 062115, doi: 10.1063/5.0096585.
[31] G. Liang, Y. Chen, L. Chen, S. Shen, Maximum spreading for liquid drop impacting on solid surface, Ind. Eng. Chem. Res., 58 (2019) 10053–10063.
[32] C. Liu, M. Shen, J. Wu, Investigation of a single droplet impact onto a liquid film with given horizontal velocity, Eur. J. Mech. B. Fluids, 67 (2018) 269–279.